Muon Neutrino Charged Current Inclusive Charged Pion ($CC\pi^{\pm}$) Production in MINERvA

B. Eberly, on behalf of the MINERνA collaboration

University of Pittsburgh, Pittsburgh, PA, USA

Abstract. The production of charged pions by neutrinos interacting on nuclei is of great interest in nuclear physics and neutrino oscillation experiments. The MINERνA experiment is working towards releasing the world's first high statistics neutrino pion production measurements in a few-GeV neutrino beam. We describe MINERνA's $CC\pi^{\pm}$ analysis event selection in both the neutrino and antineutrino beams, noting reconstruction resolutions and kinematic limits. We also show area-normalized data-simulation comparisons of the reconstructed muon and charged pion kinetic energy distributions.

Keywords: Neutrino, cross sections, pion

INTRODUCTION

Precise models of $CC\pi^{\pm}$ interactions on nuclear targets are needed to constrain certain systematic errors in neutrino oscillation experiments[1]. Many theoretical calculations model these interactions[2, 3, 4, 5, 6], but their predictions are tested primarily by hydrogen and deuterium neutrino scattering data with large uncertainties and little information on final state particle kinematics[7, 8]. For this reason, there is great interest in comparing these models to the recent high-statistics charged current single π^+ ($CC1\pi^+$) production cross section measurements at 1 GeV by MiniBooNE[9]. These comparisons indicate that the MiniBooNE data appears to favor models that do not include final state interactions (FSI)[10].

MINERνA[11], a fine-grained scintillator tracking detector that sits in the few-GeV NuMI neutrino beamline[12] at Fermilab, will measure inclusive and exclusive $CC\pi^{\pm}$ total and differential cross sections on a variety of nuclear targets. These measurements will be used to constrain $CC\pi^{\pm}$ models and will provide additional insight into discrepancies between the theory and experiment. In these proceedings, we present the status of MINERνA's measurement of inclusive $CC\pi^{\pm}$ production by muon neutrinos (ν_μ) and antineutrinos ($\overline{\nu_\mu}$) on scintillator. The signal channels for these measurements are defined to be

$$\nu_\mu A \rightarrow \mu^- \pi^{\pm} X A'$$

$$\overline{\nu_\mu} A \rightarrow \mu^+ \pi^{\pm} X A'$$

where A is the target nucleus in scintillator, A' is the recoil nucleus, and X represents any additional particles in the final state. By including the result of FSI, these definitions reduce measurement dependence on nuclear modeling, allowing for strong experimental constraints on neutrino event generators and theoretical models.

EVENT SELECTION

The ν_μ and $\overline{\nu_\mu}$ analyses presented here share almost identical reconstruction procedures and event selection criteria, differing only in the particle identification (PID) and muon charge selections. Both analyses require that the event reconstructed vertex lie within the scintillator tracker fiducial volume. The fiducial volume is chosen to minimize contamination from interactions in the passive material of the nuclear targets and calorimeters; the total contamination from such events is less than 1%. Additionally, a number of quality cuts are imposed on the muon track to remove backgrounds from neutrino interactions that occur outside of the detector.

Charged current (CC) events are identified by requiring that one of the reconstructed tracks originating from the primary vertex be matched to a reconstructed track in MINOS. This selection reduces neutral current (NC) backgrounds to a negligible amount but limits muon acceptance to greater than 2.0 GeV/c in momentum and less

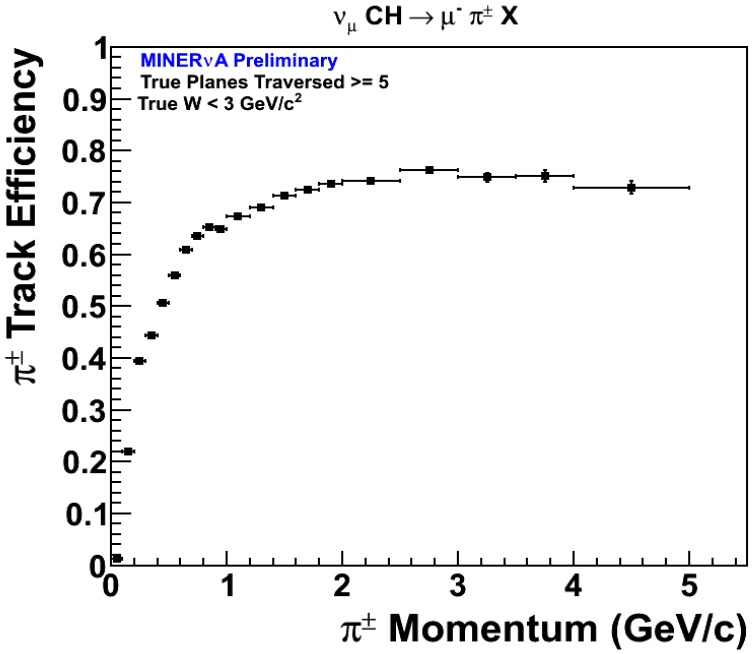

FIGURE 1. The charged pion tracking efficiency as a function of momentum.

than 20° in angle with respect to the neutrino beam. Additionally, the correct neutrino helicity is selected by requiring that the reconstructed q/p in MINOS is negative (positive) in the ν_μ ($\overline{\nu_\mu}$) analysis. These cuts reduce the combined NC, ν_e, and wrong helicity neutrino backgrounds to approximately 1% in the ν_μ analysis.

To select inclusive pion events, both analyses require that there exists at least one track at the primary vertex that is not identified as the reconstructed muon; such tracks are called hadronic tracks. The efficiency of this selection correlates strongly with the charged pion tracking efficiency. Figure 1 shows the charged pion tracking efficiency as a function of momentum. The tracking efficiency between 200-400 MeV/c is approximately 40%; this momentum range corresponds to the largest discrepancy between theoretical models and the MiniBooNE CC$\pi^\pm$ differential cross section with respect to pion kinetic energy. Though the tracking efficiency increases to almost 75% at high momentum, these high momentum tracks often do not cover the entire length of the pion trajectory. This is primarily due to secondary interactions experienced by the pion in the detector (henceforth referred to as an "interacting pion"). It is very difficult to correctly reconstruct the kinetic energy of high-momentum interacting pions, so we require that the total visible hadronic energy in the detector be less than 2.5 GeV. This removes events that are likely to contain high energy pions and effectively limits the invariant hadronic mass (W) of selected events to less than 4 GeV.

After these selections, all hadronic tracks at the primary vertex are submitted to a PID algorithm. The algorithm fits the measured energy loss (dE/dx) of each hadronic track to pion and proton hypotheses with varying momenta. The fit assumes that the particle is contained inside the inner detector, so each hadronic track is also required to be contained in the inner detector. The χ^2 of the best fit momenta for both the pion and proton hypotheses are used to calculate a pion score. The best fit pion hypothesis momentum is used as the reconstructed momentum. Figure 2 shows the pion score distribution in the ν_μ analysis. We select events with at least one hadronic track with pion score greater than 0.4.

The antineutrino analysis requires an additional PID selection, called stopping PID (SPID), which is designed to select non-interacting pions that stop in the detector's tracker region. This selection reduces the fraction of reconstructed pions with a poor reconstructed momentum. The SPID procedure compares the dE/dx profile of the end of the pion track (covering the Bragg region) to a calculated template, producing a score. Figure 3 shows the SPID score distribution in the $\overline{\nu_\mu}$ analysis. Selected events are required to have at least one pion track with stopping score greater than 0.6. This entire selection procedure yields a CC$\pi^\pm$ sample with greater than 80% purity for both analyses.

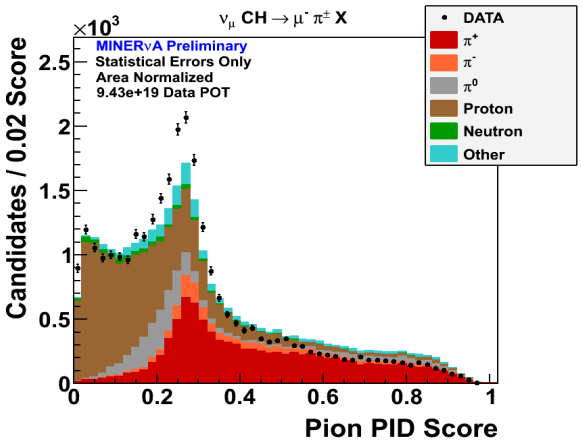

FIGURE 2. The neutrino analysis pion score distribution. The Monte Carlo simulation (MC) is area-normalized to data. Pion and proton hypotheses are equally likely at pion score = 0.3. We select tracks with pion score greater than 0.4.

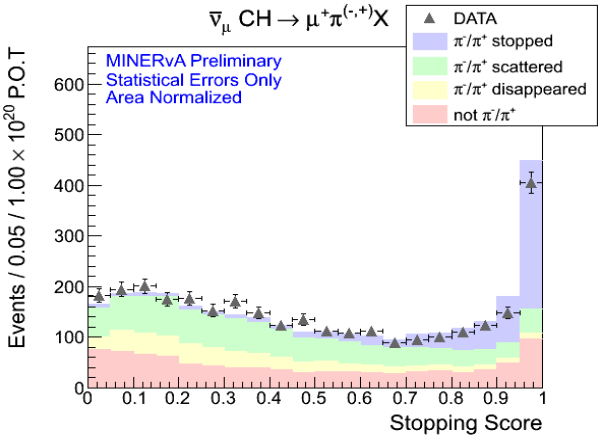

FIGURE 3. The antineutrino analysis SPID distribution. We select non-interacting ("stopped") pions by requiring that the stopping score is greater than 0.6. "Disappeared" pions are absorbed on a nucleus or converted to a π^0 before stopping.

RESULTS

The following results use approximately 25% of the available ν_μ beam interactions and almost all available $\overline{\nu_\mu}$ beam interactions in MINERνA. Figure 4 shows the reconstructed muon momentum distribution in both analyses. The data distribution is compared to a simulation that uses GENIE[13] v2.6.2 as input. In the ν_μ analysis, the simulated distribution includes error bands with the shape components of the GENIE and beam flux systematic errors. The muon momentum and angular resolutions are approximately 5% and 0.7°, respectively.

Figure 5 shows the reconstructed pion momentum distribution in both analyses. The pion angular resolution is about 2°. The reconstructed momentum resolution is 10-15% for non-interacting pions, but can be much larger for those that interact. The SPID cut, which tends to select lower energy pions, is primarily responsible for the shape difference between the two analyses. The flat region at 200 MeV in the ν_μ distribution is an artifact of the PID procedure that has since been remedied.

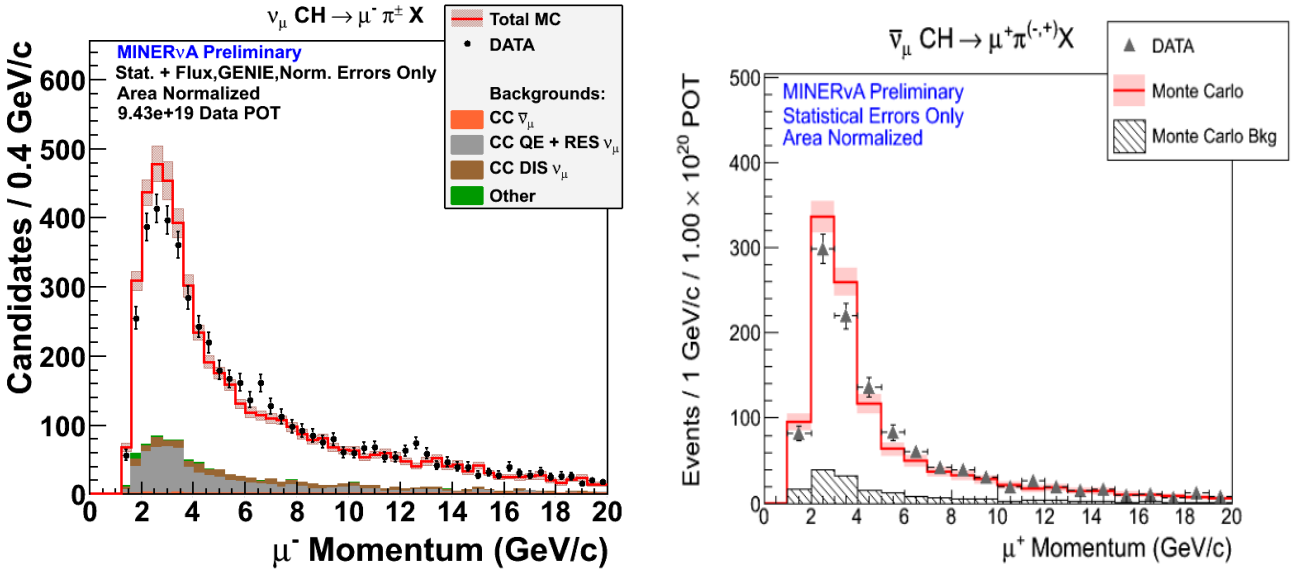

FIGURE 4. Reconstructed muon momentum distributions.

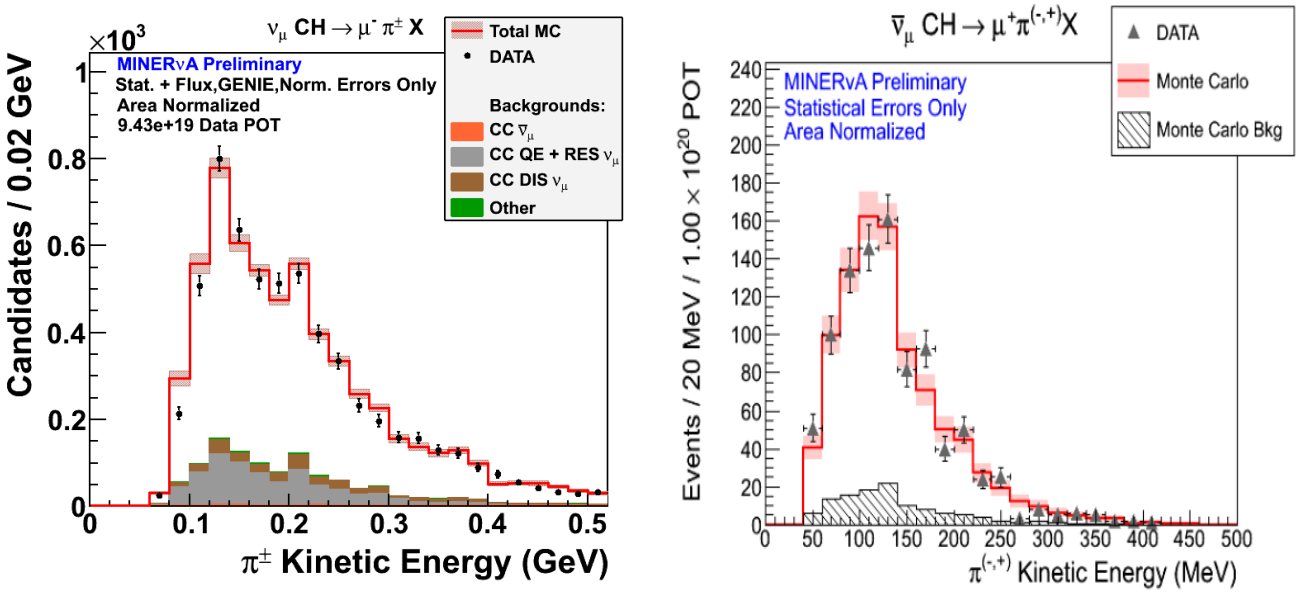

FIGURE 5. Reconstructed charged pion kinetic energy distributions.

CONCLUSIONS

MINERνA is well-suited and dedicated to providing a full suite of inclusive and exclusive CC$\pi^\pm$ cross section measurements on multiple nuclear targets. These measurements will be very useful in evaluating theoretical models while also providing insight into the current tension between models and experiment. We have shown here the status of two inclusive CC$\pi^\pm$ measurements in MINERνA, presenting an event selection that yields a reconstructed pion sample with greater than 80% purity.

This analysis will be advanced by using calorimetrically-reconstructed hadronic energy to improve the pion kinetic energy measurement and produce measurements of E_ν, Q^2, and W. Additionally, we are implementing background

subtraction, detector resolution unfolding, and efficiency corrections, while also developing procedures to evaluate systematic errors related to hadron reconstruction.

ACKNOWLEDGEMENTS

Thank you to Helio Motta and Jorge Morfin for organizing this conference and the invitation to present this work. Also, thank you to Cliff Simon for his leadership on the $\overline{\nu_\mu}$ analysis and to Steve Dytman for his unwavering mentorship and patience. The author's work on MINERνA is supported by the Department of Energy Grant Number DE-FG02-12ER41832.

REFERENCES

1. D. A. Harris *et al.* (2004), arXiv:hep-ex/0410005.
2. E. A. Paschos and Dario Schalla (2012), arXiv:1212.4662[hep-ph].
3. M. Sajjad Athar, S. Chauhan, and S. K. Singh, J. Phys. **G37**, 015005 (2010).
4. M. Martini, M. Ericson, G. Chanfray, and J. Marteau, Phys. Rev. **C80**, 065501 (2009).
5. E. Hernandez, J. Nieves, M. Valverde, and M. J. Vicente Vacas, Phys. Rev. **D81**, 085046 (2010).
6. O. Lalakulich, K. Gallmeister, and U. Mosel, Phys. Rev. **C86**, 014607 (2012).
7. S. J. Barish *et al.*, Phys. Rev. **D19**, 2521 (1979).
8. T. Kitagaki *et al.*, Phys. Rev. **D34**, 2554 (1986).
9. A. A. Aguilar-Arevalo *et al.*, Phys. Rev. **D83**, 052007 (2011).
10. U. Mosel and O. Lalakulich (2012), arXiv:1211.1977[nucl-th].
11. A. Fiorentini, "The MINERνADetector", these proceedings (2012).
12. "The NuMI Technical Design Handbook", `http://www-numi.fnal.gov/numwork/tdh/tdh_index.html` (2004).
13. C. Andreopoulos *et al.*, Nucl. Instrum. Meth. **A614**, 87-104 (2010).